Desalination and Water Treatment
www.deswater.com

doi: 10.5004/dwt.2020.26434

207 (2020) 398–409
December

Removal of methylene blue with nanomagnetic coated wild chestnut shells: thermodynamic, kinetic, isotherm, and mechanism studies

Esra Altıntıg, Meryem Daglar, Huseyin Altundag*

Department of Chemistry, Faculty of Arts and Sciences, Sakarya University, Sakarya, Turkey, emails: altundag@sakarya.edu.tr (H. Altundag), altintig@sakarya.edu.tr (E. Altıntıg), mrymdglr1@gmail.com (M. Daglar)

Received 18 February 2020; Accepted 4 August 2020

ABSTRACT

Adsorption is one of the important methods used to remove dyestuff (methylene blue) from industrial wastewaters with suitable adsorbents. In this study, magnetic wild chestnut shell coated Fe_3O_4 was used as the adsorbent. The magnetic wild chestnut shell coated Fe_3O_4 nanoparticles were synthesized using the chemical precipitation method. The surface properties of the adsorbents were characterized by using spectroscopic techniques such as scanning electron microscopy, X-ray diffraction, Brunauer–Emmett–Teller, and Fourier transform infrared spectroscopy. The effect of adsorption parameters such as initial pH (2–9) value, adsorbent dosage (0.1–0.5 g), temperature (298–318 K), contact time (0–240 min), and initial concentration (25–150 mg L^{-1}) were researched. The experimental data indicated that the adsorption isotherms were well described by the Langmuir equilibrium isotherm equation and the calculated adsorption capacities of the magnetic wild chestnut shell coated with Fe_3O_4 were 140.84 mg g^{-1}. The adsorption of methylene blue was determined as in compliance with the pseudo-second-order kinetic model. The thermodynamic parameters calculated to estimate the nature of adsorption indicated spontaneous and endothermic adsorption ($\Delta H°$ = 69.00 kJ mol^{-1}). The adsorption/desorption circulation test showed good reusability performance up to the fourth cycle. Furthermore, considering all the results, the advantage of being produced from a cheap source, high adsorption capacity, and rapid procurement feasibility has led to a great promise for the removal of methylene blue from aqueous solutions.

Keywords: Magnetic chestnut; Fe_3O_4; Methylene Blue; Adsorption; Desorption

1. Introduction

Wastewater from industrial sectors such as cosmetics, textile, dyeing, printing, food, and the paper was contaminated with dyestuffs. During the dyeing process, approximately 50% of the reactive dyestuffs used end up in wastewater [1]. Dyestuff in wastewater causes significant environmental problems due to toxic effects on aquatic life and affecting photosynthetic activity in aquatic life by reducing light transmittance [2,3]. Dyestuffs lead to the formation of toxic and carcinogenic products as the result of accumulation in organisms. Dyestuffs are generally grouped as anionic, cationic, and non-ionic [2]. Methylene blue (MB) is important because it is a model compound for the measurement of dying adsorption capacity of the adsorbents at the same time and their wide use in various sectors among the dyestuffs. This dyestuff called as MB which is also known as tetramethyl thionine, can be easily oxidized. It is a cationic dyestuff which is used particularly in the textile industry, and generally has toxic and carcinogenic effects and can cause cancer, mutations, and dermatological diseases [4]. Physical, chemical, and physicochemical processes are being applied for the removal of the dyestuffs

* Corresponding author.

from wastewaters. The treatment technologies required to be applied are determined by considering the qualitative and quantitative characteristics of wastewater. For the treatment of wastewater, various methods are applied such as ion exchange, chemical precipitation, reverse osmosis, membrane filtration, and adsorption. The adsorption method is a very effective and economical technique that has been studied in recent years because it is quite stable among the methods used for the removal of pollutants [5]. Fulfillment of adsorption processes at a reasonable cost can only be possible by the use of abundant, easily available adsorbents with low production costs. Although the most commonly used adsorbent in the adsorption method is activated carbon [6], clays such as zeolite, bentonite, montmorillonite, sepiolite [7], pumice [8], agricultural and fermentation wastes [9], coal [10], fly ash [11], sawdust and sand [12], fruit wastes, apricot kernels, corn cobs, peanut shells, rice shells, and other agricultural wastes [13–15] have also been tried and achieved success in color removal at varying levels. All of the materials used have important advantages such as being easily accessible, locally applicable and having a reasonable cost. In recent years, there are quite a lot of studies on this subject. The researchers investigated the effects of pH, contact time, temperature effect, absorbent concentration, and ionic strength on adsorption [16]. Among the inorganic minerals in the environment, iron oxide minerals which are present as separate particles and coatings in other mineral particles with a large surface area, have the most reactive surface areas capable of binding both natural inorganic and organic pollutants including cations and anions. Iron oxides generally affect the distribution of free metal concentration and natural organic substances due to interfacial processes in aqueous dispersions. Its adsorption on different absorbent materials such as chromium, iron, iron oxide, iron-coated sand and iron-coated activated carbon [17], and granular ferric hydroxides [18] has also been investigated. One of the most important magnetic materials with strong electrical and magnetic properties is Fe_3O_4. Superparamagnetism is one of the most important features when the Fe_3O_4 particle size is smaller than the critical diameter [19]. Magnetite nanoparticles (Fe_3O_4) obtained for this purpose can be used as a surface coating in the adsorption processes to increase the surface area of the adsorbent. Magnetic nanoadsorbents such as Fe_3O_4 at chip carbon and EDTA at Fe_3O_4 at chip carbon [20], $ZnFe_2O_4$ modified with sodium dodecyl sulfate [21], and Fe_3O_4 loaded active corncob [22] can be used as nanoadsorbents recently. It is clear by these studies that surface changes increased the physical and chemical characteristics of nanoadsorbents, by the way it is seen by the studies that it has become more useful on the removal of the dyestuffs from the wastewaters [20].

In this study, wild chestnut shells were coated with Fe_3O_4 magnetite nanoparticles to increase the possibility of adsorption. To better understand the adsorption mechanism, magnetically charged adsorbents were analyzed by Fourier transform infrared spectroscopy (FT-IR), X-ray diffraction (XRD), and scanning electron microscopy/energy-dispersive X-ray spectroscopy (SEM/EDS) techniques before and after the adsorption process. The data have been evaluated with adsorption isotherm model, kinetics, and thermodynamic equations.

2. Materials and methods

2.1. Material

The wild chestnuts used in the research have been collected around the Sakarya Region. Outer shells of wild chestnut have been rinsed by pure water three times and dried at 100°C for 24 h. The dried shells have been squashed and crumbled to a size of less than 4 mm with the help of a press. The cationic dyestuff; Methylene blue (MB) with the formula ($C_{16}H_{18}ClN_3S$) having a molecular weight of 319.85 g moL^{-1} was purchased from a commercial supplier. The chemical structure of MB is shown in Fig. 1. The mixing of chemical substances was performed by IKA KS 501 orbital shaker. METTLER TOLEDO (Colombus, Ohio, ABD) pH meter was used for pH measurements of solutions and BLULAB drying chamber was used for drying processes. All chemicals with analytical grade, NaOH, HCl, MB, $FeSO_4{\cdot}7H_2O$, and $FeCl_3{\cdot}6H_2O$ (Merck), it was supplied from Germany.

2.2. Preparation of the Fe_3O_4-WC

$FeSO_4{\cdot}7H_2O$ and $FeCl_3$ solution were added into a 400 mL beaker. After heating solution to 70°C on a heater, 3.3 grams of wild chestnuts (WC) was weighed and added to the mixture. One-hundred milliliters of 5 M NaOH were added to this mixture to precipitate iron oxide. After adjusting to pH 10 with NaOH, it has been allowed to stir for 3 h at 80 rpm at 50°C. The composite material was washed with distilled deionized water and filtered. The magnetic properties of WC-Fe_3O_4 were determined by preliminary experiments using a neodymium magnet [23]. Fig. 2 shows the magnetic response of Fe_3O_4-WC to an external magnetic. The synthesis schema of the Fe_3O_4-WC sorbent is is illustrated in Fig. 3.

2.3. Characterization

The SEM/EDS analysis were studied with JEOL JSM-6060 LV model instrument under a high vacuum at 20 kV. FT-IR spectroscopy (SHIMADZU IR Prestige 21, Kyoto, Japan) was used for the analysis of the functional groups present on the surface of WC, before and after MB adsorption. The absorbance values of the functional groups in the structure of the molecule were analyzed in the wavelength range of 400–4,000 cm^{-1}. XRD patterns were obtained at room temperature by RIGAKU D/Max2200 XRD, using CuKα radiation (λ = 1.5406 Å). Diffraction method (XRD) is based on breaking X-rays in each crystalline phase depending on their unique atomic sequence. It is based on breaking the X-rays in a characteristic order. Sample was analyzed in the range of 10°–80° in the points located between 2θ angles. The surface area, which is the specific feature of WC, pre-adsorption, and post-adsorption samples, was measured by applying

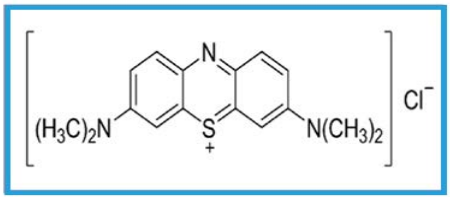

Fig. 1. Molecular structure of MB, λ_{max} = 665 nm.

the Brunauer–Emmett–Teller (BET) equation to the adsorption–desorption isotherm of N_2 at 77 K. The surface area and pore value of the WC, WC-Fe_3O_4, and WC-Fe_3O_4-MB were measured by MICROMERITIC brand Accelerated Surface Area and Porosimetry System, (Norcross , Georgia, USA). Absorbance measurements were carried out using Shimadzu UV-2700 spectrophotometer, (Kyoto, Japan) in the range of 400–800 nm.

2.4. Adsorption experiments

Stock solution of Methylene blue (MB) was prepared at a concentration of 1,000 mg L^{-1}. Standard solutions (1–5 mg L^{-1}) and working solutions (25–250 mg L^{-1}) were prepared from stock solutions by diluting with deionized water (chemical resistance: 18 MΩ cm). The pH of the solution has been adjusted with 1.0 M HCl and 1.0 M NaOH.

Ultraviolet and visible light (UV-vis) measurement on a Shimadzu UV-2600 spectrophotometer, (Kyoto, Japan) brand device is the measurement of the reduction of a beam after it has passed through a sample or reflected from a sample surface. The measurement wavelength was determined as 665 nm. The deionized water as a solvent, and quartz tubs were used. The effects of the following parameters are determined separately in the written range: contact time (10–640 min), initial dye concentration (25–250 mg L^{-1}), adsorbent dose (0.1–0.5 g), pH values (2–9), process temperature (298–318 K). Then the optimum values during adsorption experiments were determined separately. It has been initiated the effect of the pH of the solution in the analysis.

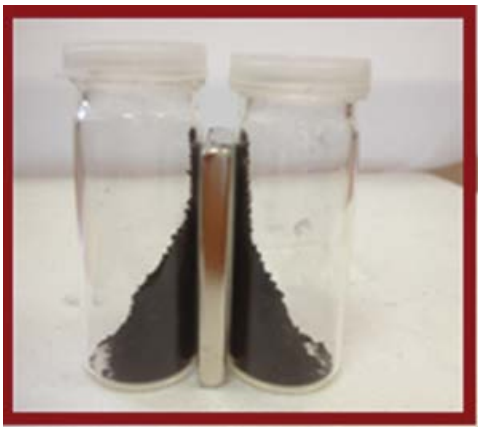

Fig. 2. Magnetic response of Fe_3O_4-WC to an external magnetic.

WC contains negative sites (O_2 and OH) that interact with positively charged ions. Similarly, Fe_3O_4 nanoparticles also having lots of available O_2 sites around Fe^{+2} and Fe^{3+} atoms that interact with the positive sites of the cationic MB dye. Furthermore when we use iron oxide nanoparticles loaded WC, then we get more negatively charged active sites for the experimental system of basic dyes removal which enhances the interaction among adsorbent and adsorbate surface hence, there is an increase in removal percentage and adsorption capacity for MB removal by synthesized [22]. Fig. 4 shows the possible adsorption mechanism for dye removal onto WC-Fe_3O_4.

When the adsorption process has reached equilibrium, the amount of material adsorbed by the unit mass of the adsorbent material is a function of its temperature, concentration, pressure, and equilibrium pressure. The adsorbed yield of the MB (%) and its adsorbed amount per adsorbent unit mass have been determined by applying the following equation:

As soon as the system comes to equilibrium during the adsorption process, this function is equal to the following equation, where the temperature is kept constant:

$$q_e = \frac{\left(C_0 - C_e\right)}{m} \times V \tag{1}$$

$$\text{Removal}\left(\%\right) = \frac{\left(C_0 - C_e\right)}{C_0} \times 100 \tag{2}$$

where q_e is equilibrium concentration of adsorbed MB onto Fe_3O_4-WC (mg g^{-1}). C_0 and C_e is initial (mg L^{-1}) and equilibrium concentration of MB in the solution at equilibrium time (mg L^{-1}), respectively. V and m are solution volume (mL) and weight of the adsorbent (g), respectively. q_e is the adsorption capacity of adsorbent (mg g^{-1}), C_0 is the MB initial concentration (mg L^{-1}), C_e is the concentration of adsorbent (adsorbed material) at equilibrium

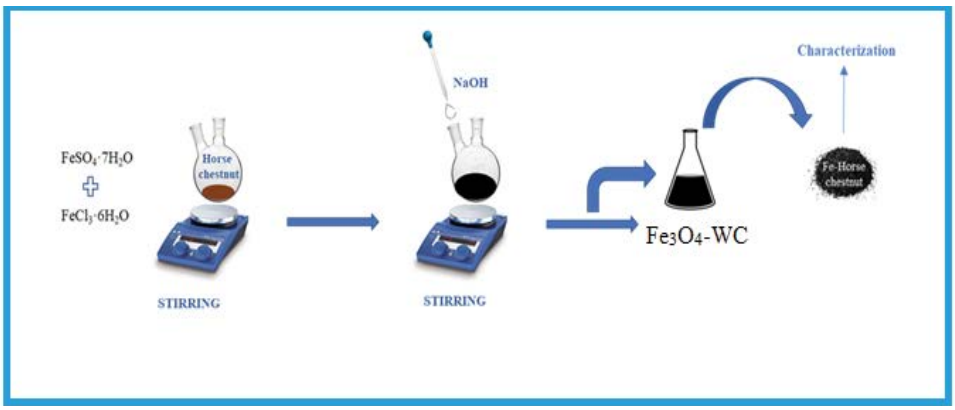

Fig. 3. Schematic representation of the magnetization of wild chestnut shell.

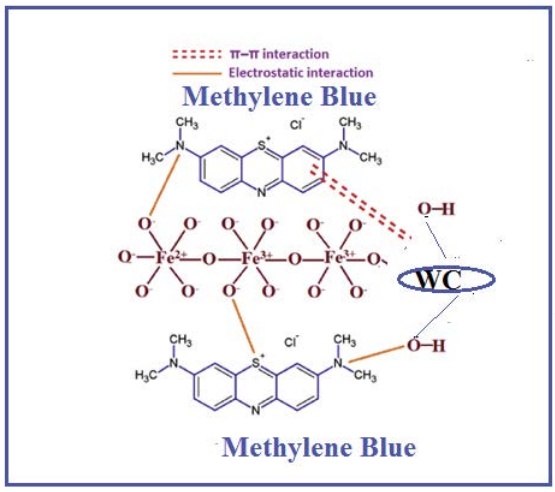

Fig. 4. Adsorption mechanism for MB removal onto WC-Fe_3O_4.

(remaining from adsorption process) (mg L^{-1}), V is the volume of solution (L), m is the weight of adsorbent (g).

2.5. Regeneration studies

In the adsorption–desorption studies performed to determine the reusability of the adsorbate, firstly, the adsorption cycle was carried out. For the adsorption–desorption process, the dyestuff solutions (25 mg L^{-1}, pH 7.0) were washed with 0.1 g of adsorbate and stirred at 130 rpm for 1 h. After completion of each adsorption study, the solid portion separated from the liquid portion was washed with distilled water before being dried in an oven at 60°C overnight for the next desorption study. The adsorption–desorption cycle was performed seven times. The amount of desorption (D%) was based on the amount adsorbed (C_a; mg g^{-1}) and the desorbed amount C_d (mg g^{-1}) according to the following equation.

$$\text{Desorption}\left(D\%\right)=\frac{C_d}{C_a}\times 100 \tag{3}$$

3. Results and discussion

3.1. Characterization result

Textural parameters of WC, Fe_3O_4-WC, Fe_3O_4-WC-MB sorbents are given in Table 1.

The magnetite particles caused a significant increase in the surface and micropore areas of the WC after loading. Also, the magnetic particles loaded into the WC caused a slight increase in their median pores and average pore widths. The result showed that Fe_3O_4 coated on the surface of the Fe_3O_4-WC made a difference in the removal of MB.

EDS analysis were conducted by benefiting from SEM image in order to obtain element structure of element Fe_3O_4-WC. SEM/EDS imaging that was obtained for Fe_3O_4-WC sorbent is given in Fig. 5.

The surface of Fe_3O_4-WC in the EDS images contains Fe and O elements caused by Fe_3O_4 sorbent. C, Mg. Na and P are also found by the structure of WC. Si was come from the soil and existed in the structure with trace amounts. Surface morphology as well as shape and size of particles were determined according to SEM images and information about elemental analysis was determined according to EDS.

The porous structure of the particles on the outer shell of the raw wild chestnut was seen in some zoomed images of Fe_3O_4-WC particles before MB adsorption and Fe_3O_4-WC particles after MB adsorption, which was obtained by using the SEM technique.

When the SEM image of the wild chestnut outer shell shown in Fig. 6a was examined, a smooth structure was observed. The dotted whiteness shown in the Fe_3O_4-WC SEM images in Fig. 6b indicates the presence of iron. In Fig. 6c, when the SEM images of MB were analyzed after MB adsorption, it was observed that MB was attached to the porous surface of the wild chestnut and to the inside of the particles. This shows that the adsorption was carried out successfully. XRD analysis was performed to determine the crystalline structure of the powdered samples belonging to the wild chestnut covered by Fe_3O_4-WC and dyestuff. The diffraction patterns obtained are given in Fig. 7 by the XRD spectrum.

In Fig. 7a, the 2θ characteristic reflection peak where the XRD spectrum was examined was seen at 22.05°. Thanks to these peaks, it was understood that WC was in an amorphous structure. When the XRD spectrum of Fe_3O_4-WC nanocomposites is examined in Fig. 7b, characteristic reflection 2θ peaks were seen at 18.14°, 35.06°, 42.74°, 53.02°, 61.05°, and 70.09°. Similar studies can be found in the literature [23]. When the powder XRD spectrum of Fe_3O_4-WC nanocomposites with MB shown in Fig. 7c were examined, characteristic reflection 2θ peaks are given in Fig. 7c. It is seen that these peaks observed after activation by MB have an amorphous structure. No characteristic peak was observed after activation.

Table 1
Textural data of WC, Fe_3O_4-WC, and Fe_3O_4-WC-MB sorbents

Textural parameter	WC	Fe_3O_4-WC	Fe_3O_4-WC-MB
BET surface area (S_{BET}) (m^2 g^{-1})	187.21	522.54	376.32
Langmuir surface area (m^2 g^{-1})	236.83	754.21	448.23
Micropore area (m^2 g^{-1})	87.76	224.52	124.57
Median pore width (nm)	2.06	2.24	2.46
BJH average pore width (4 V/A) (nm)	3.67	4.21	4.53
t-plot external surface area (m^2 g^{-1})	93.46	614.75	227.46

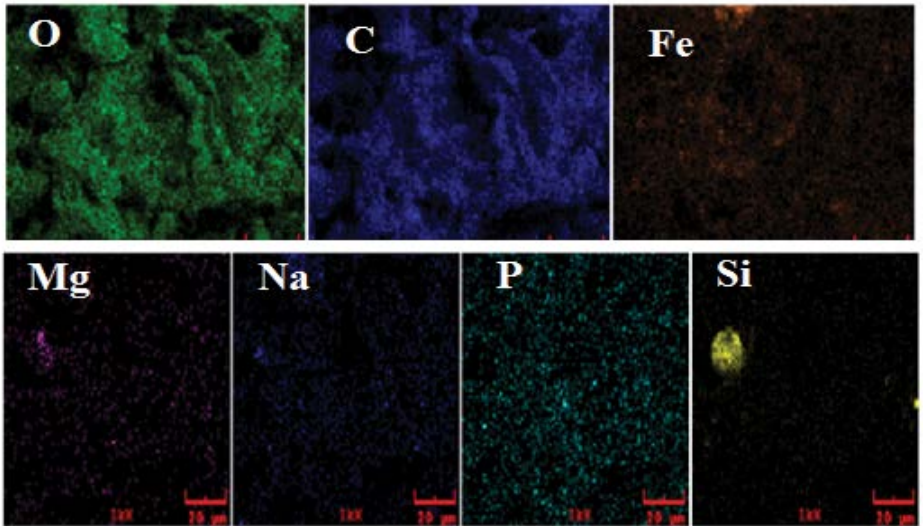

Fig. 5. SEM/EDS results obtained for the Fe_3O_4-WC composite.

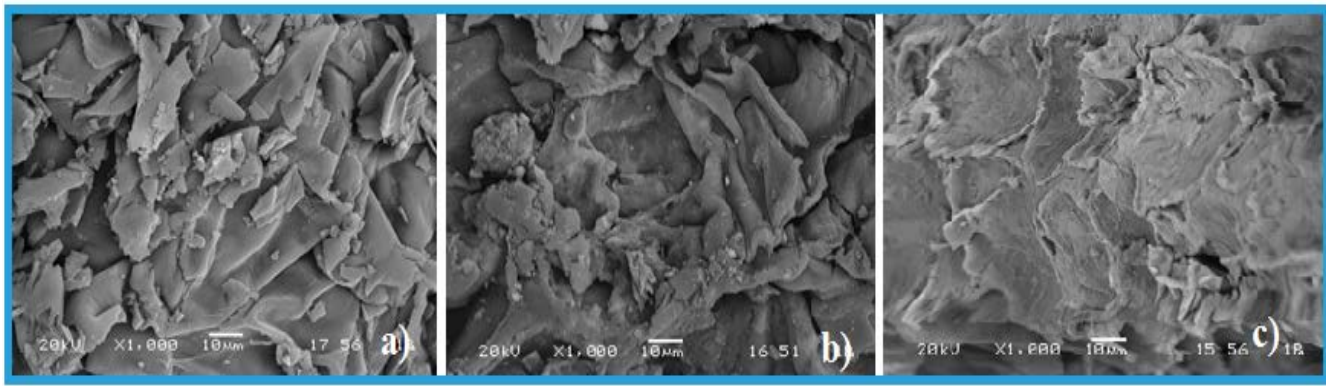

Fig. 6. SEM photographs of (a) WC, (b) Fe_3O_4-WC composite, and (c) Fe_3O_4-WC composite after the adsorption.

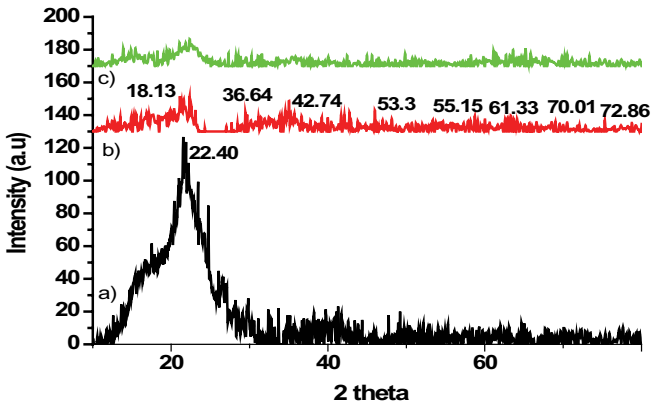

Fig. 7. XRD diffraction patterns of (a) WC, (b) Fe_3O_4-WC composite, and (c) Fe_3O_4-WC composite after the adsorption.

FTIR spectroscopy analysis was performed in the range 4,000–400 cm^{-1}. Fig. 8a corresponds to the tensile vibration of band [OH] groups seen around 3,500 cm^{-1} [24]. Peaks at the region of 1,750 cm^{-1} indicate that aromatic C=C tensions were absorbed in this region. In addition, small peaks between the wave numbers in the range of 1,150–1,280 cm^{-1} correspond to the C–OH and O–H tensions of alcohols and in the phenolic groups [24]. 500–750 cm^{-1} adsorption bands seen in Fig. 8b were corresponded to Fe–O vibration [25]. In our study, the band seen around 560 cm^{-1} in the Fe_3O_4-WC and Fe_3O_4-WC-MB samples were Fe–O vibration band. When the results obtained for Fe_3O_4-WC-MB sample are examined in Fig. 8c, it was observed that there was a significant decrease in the O–H stress peak seen around 3,500 cm^{-1} as a result of activation and carbonization interaction. The reason for this change was primarily due to the removal of water in biomass interaction with carbonization. No significant change was observed in other basic peaks of biomass.

3.2. Effects of pH and adsorbent dosage on the adsorption yield of MB onto WC

pH was one of the most important parameters that control the adsorption of the dye on the particles in the surfaces of the solid substance [26]. It affected not only

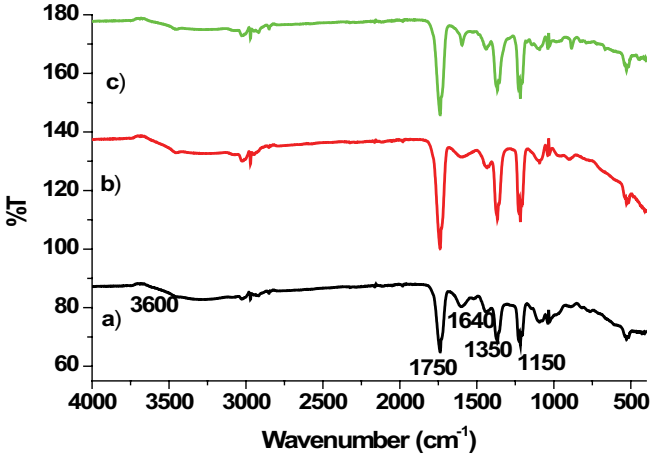

Fig. 8. FTIR spectrums of (a) WC, (b) Fe_3O_4-WC composite, and (c) Fe_3O_4-WC composite after the adsorption.

the degree of ionization of adsorbates but also the surface charges of adsorbents [24].

In order to investigate the effect of pH effect (%) on Fe_3O_4-WC sorbent, MB solutions were prepared at initial pH values ranging from 2.0 to 9.0, concentration of 25 and 50 mg L^{-1} and at 298 K. The data for the MB removal effect of pH are shown in Fig. 9.

To determine the effect of pH the adsorption of MB, 25, and 50 mg L^{-1} adsorbent concentrations were studied. As there were not much difference between them, the process was continued with 0.1 g. Different initial concentrations adsorbents were added to the adsorbate solutions which were adjusted to optimum pH values and mixed in the magnetic stirrer for 240 min. The solid and liquid phases were separated by centrifugation and the dyestuff has been determined by UV spectroscopic method in the liquid phase.

It is seen that the adsorption of MB increases with increasing solution pH. This is probably due to the excess OH^- ion in the environment and the cationic structure of the dyestuff. At basic pH, it was thought that excess OH^- ions in the environment create complex with cationic dyestuff and decrease adsorption [26]. The MB adsorption was higher than the adsorption at acidic pH where the pH concentration is ≥7.

3.3. Effect of the mixing time on the adsorption yield

In line with the results obtained from the experimental data, the adsorption value was increased with increasing time and, after a certain period, the dyestuff retention rate came to the equilibrium. Fig. 10 shows a removal efficiency (%) in terms of the change in mixing time.

As can be seen from Fig. 10, the adsorption efficiency (%) shows a linear increase with increasing mixing time for both concentrations and then remains constant. After the equilibrium period, a yield of more than 96% was obtained for the substance at a concentration of 50 mg L^{-1} and a yield close to 90% for the substance at 25 mg L^{-1} concentration, and equilibrium was reached after 360 min. Therefore, it was defined as kinetic modeling of optimal time and equilibrium adsorption for the next study. As a result, the effect of mixing time on adsorption was determined as 360 min.

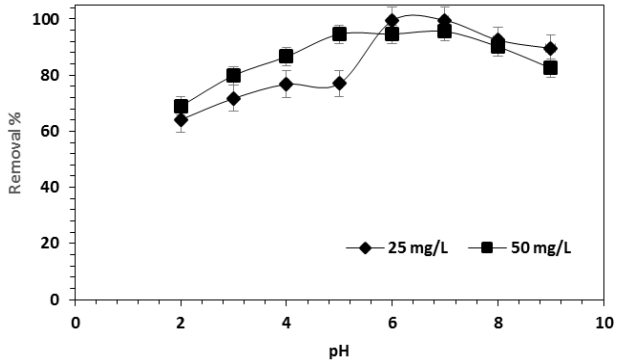

Fig. 9. Effect of MB removal yield on the pH of the solution (initial MB concentration: 25, 50 mg L^{-1}, temperature: 298 K, and adsorbent dose: 0.1 g/100 mL).

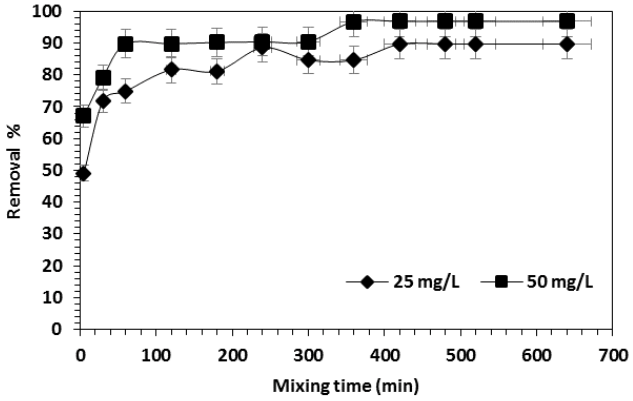

Fig. 10. Mixing time effect the removal yield of MB (temperature: 298 K and pH: 7.0).

3.4. Effect of adsorbent dose effect on the adsorption yield

The effect of adsorbent dose over the removal of MB was researched by using 10 mL dye solution with 25 and 50 mg L^{-1} dye concentration for 240 min contact time at room temperature. Adsorbent dose was changed between 0.1 and 0.4 g (Fig. 11). Adsorbent amount that will be added to the solution are among the important factors that effects the yield of the adsorbed dyestuff amount. In case of lower adsorbent amount that will be used, maximum adsorption yield to have occurred may decrease. In case of adding too much adsorbent to the solution, flocculation occurs in the solution and may affect the adsorption yield negatively [27].

As observed from the curves, the removal percentage of the dyestuff was decreased as the adsorbent amount was increased. As there is not any difference between 0.1 and 0.2 g, the study was continued with 0.1 g. This is because dyes have more active zones over the adsorbent surface for the dye adsorption at the lower concentration. This is because dyes have more active zones over the adsorbent surface for the dye adsorption at the lower concentration. In the higher dye concentrations, the percentage of the removal were lower because of the saturation of the binding points with dye molecules [23,27].

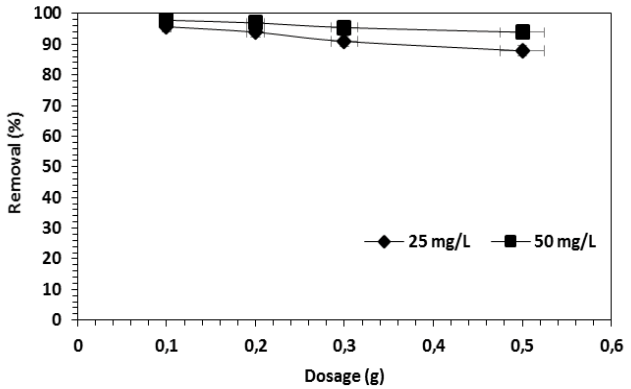

Fig. 11. Adsorbent dose effect on the removal yield of MB (temperature: 298 K and pH:7.0).

3.4.1. Adsorption isotherms

Correlations or curves showing the relationship between the equilibrated amount of adsorbate adsorbed on the adsorbent surface at constant temperature and the concentration of the adsorbate in the solution phase were called as adsorption isotherms. Adsorption isotherm is very important both theoretically and practically. In this study, Freundlich and Langmuir adsorption isotherms were used to analyze experimental data. The applicability of isotherm equations to experimental data were evaluated using correlation coefficients [27,28]. Figs. 12 and 13 with the isotherm constants being obtained from the slope.

All correlation coefficients and other isotherm constants calculated for both equations are listed Table 2. The thermodynamic parameters obtained for the adsorption of MB are given in Table 3. The correlation coefficients obtained from the Langmuir equation were higher than those obtained from the Freundlich equation. While the Langmuir R^2 value at 298 K was 0.97 and the Freundlich R^2 value was 0.59. Similarly, depending on the increase in temperature, the Langmuir R^2 value at 303 K is 0.99, while the Freundlich R^2 value was 0.94. The Langmuir R^2 value at 308 K was again 0.99, while the Freundlich R^2 value was 0.80. Considering these results, it was concluded that MB adsorption on the outer shell of wild chestnuts was more compatible with Langmuir model [28,29]. Langmuir equation and the maximum adsorption capacity of WC for MB was calculated as 140.84 mg g^{-1}.

3.5. Effect of temperature on the adsorption yield

The effect of temperature on MB adsorption between 298 and 328 K temperatures was studied by using 0.1 g wild chestnut outer shell and MB solutions at a concentration of 100 mg L^{-1}.

Fig. 14 shows the effect of temperature on MB adsorption. It was observed that the adsorbed amount of MB on the outer shell of WC increases with increasing temperature. This was due to an increase in the movement (depending on the increasing temperature) of large voluminous MB molecules, which were more stable at low temperatures [30]. This shows that MB adsorption is endothermic [31].

3.6. Thermodynamics parameters of the adsorption

The effect of temperature on MB adsorption between 298 and 318 K was studied using 0.1 g iron-coated WC outer shell and MB solutions at a concentration of 100 mg L^{-1}.

$$\Delta G^\circ = -RT \ln K_d \tag{4}$$

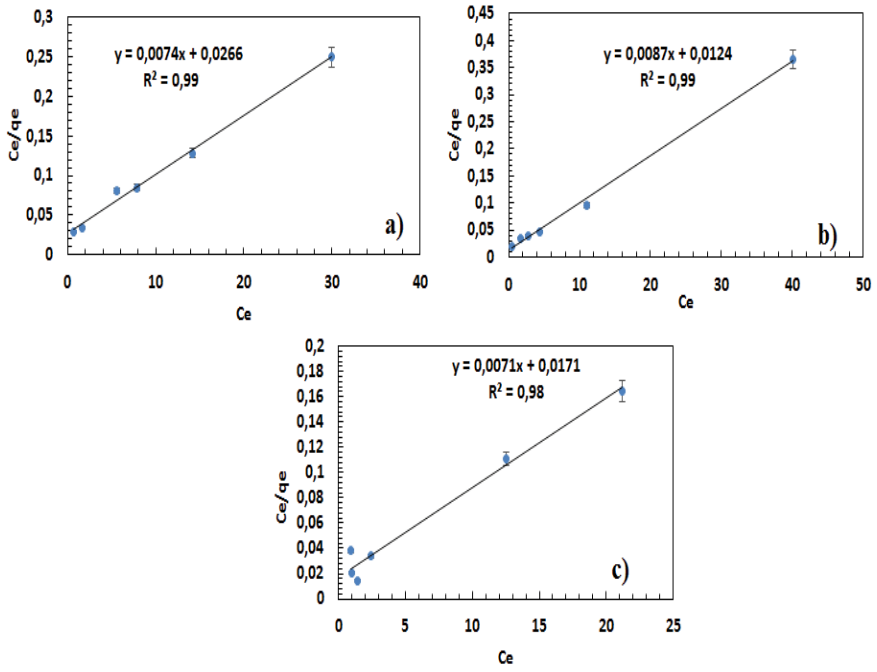

Fig. 12. (a–c) Langmuir isotherm plots obtained for the adsorption MB onto WC (MB concentration: 100 mg L^{-1}, temperature: 298 K, and adsorbent dosage: 0.1 g L^{-1}).

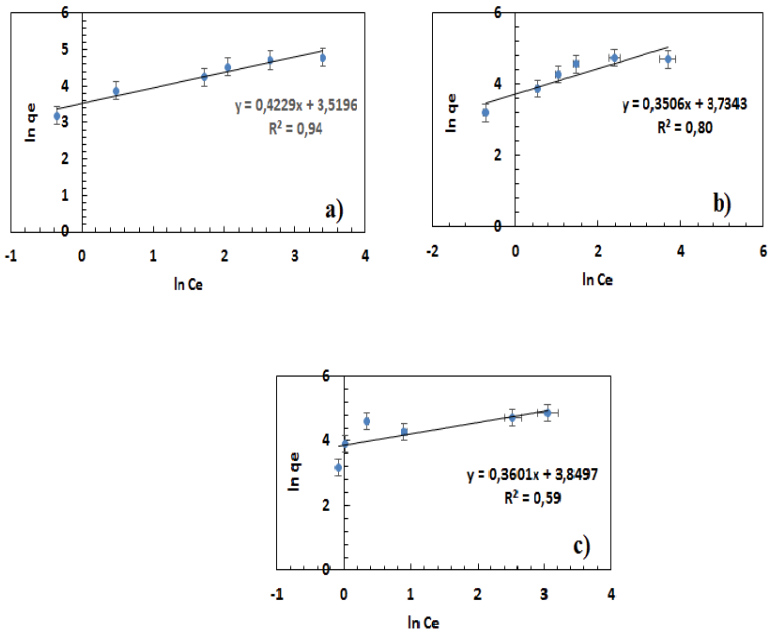

Fig. 13. (a–c) Freundlich isotherm plots obtained for the adsorption MB onto WC (MB concentration: 100 mg L^{-1}, temperature: 298 K, and adsorbent dosage: 0.1 g L^{-1}).

Table 2
Freundlich and Langmuir isotherm constants for MB adsorption

Temperature (K)	Sample	Langmuir isotherms			Freundlich isotherms		
		q_m (mg g^{-1})	b (L mg^{-1})	R^2	K_F	n (L mg^{-1})	R^2
298	Fe_3O_4-WC	140.84	0.41	0.97	24.2	2.7	0.59
308	Fe_3O_4-WC	135.13	0.27	0.99	19.1	2.3	0.94
318	Fe_3O_4-WC	114.94	0.70	0.99	35.0	2.8	0.80

Table 3
Termodynamic parameters for the adsorption of MB onto Fe_3O_4-WC

Sample	T (K)	$\Delta G°$ (kJ mol^{-1})	$\Delta H°$ (kJ mol^{-1})	$\Delta S°$ (J mol^{-1} K^{-1})
	298	–6.17		
Fe_3O_4-WC	308	–8.04	69.00	0.25
	318	–11.23		

$$K_d = \frac{q_e}{C_e} \tag{5}$$

$$\ln K_d = \frac{\Delta S°}{R} - \frac{\Delta H°}{RT} \tag{6}$$

$$\Delta H° = \Delta H° - T\Delta S° \tag{7}$$

Adsorption data $\Delta G°$ indicated that the values were negative at all temperatures, confirming the spontaneous nature of adsorption. $\Delta G°$'s positive value indicated that the adsorption process was endothermic. In other words, the applicability of the adsorption process can be understood by the fact that enthalpy and Gibbs free energy were negative. Positive $\Delta S°$ values indicated that increased coincidence of adsorbent at the solid–liquid interface during adsorption [11,32].

Whether adsorption occurs spontaneously depends on Gibbs free energy, and a negative value of $\Delta G°$ indicated that adsorption was spontaneous [33]. In addition, an increase in the $\Delta G°$ value depending on the increasing temperature indicated that MB was more adsorbed at high temperatures. A positive value of $\Delta H°$ indicated that the adsorption was endothermic. Standard entropy values ($\Delta S°$) were found to be positive for all temperatures. A positive value of $\Delta S°$

indicated that there may be a structural change between the adsorbent and the dyestuff.

3.7. Comparison of adsorption capacity of the developed magnetic adsorbent for MB removal

Table 4 shows the comparison of the adsorption capacity of these sorbents with different sorbents in the literature [11,34–40].

3.8. Adsorption kinetics

Kinetic mechanism of MB in the adsorption of the Fe_3O_4-WC adsorbent was determined by pseudo-first and pseudo-second-order kinetic models.

Equation in the pseudo-first-order equation:

$$\ln\left(q_e - q_t\right) = \ln q_e - k_1 t \tag{8}$$

where q_e is the amount of adsorbed material per gram of adsorbent at equilibrium (mg g^{-1}), q_t is the amount of adsorbed material per gram of adsorbent at any time (mg g^{-1}), t is the contact time (min), and k_1 is the speed constant.

Equation in the pseudo-second-order equation:

$$\frac{t}{q_t} = \left[\frac{1}{k_2 q_e^2}\right] + \left(\frac{1}{q_e}\right) t \tag{9}$$

where k_2 is the pseudo-second-order equation constant (g), t is the specified time constant (min), q_t is the amount of adsorbed material at the end of a t time period (mg g^{-1}), q_e is the amount of adsorbed material at equilibrium (mg g^{-1}). The values $\Delta H°$ and $\Delta S°$ were evaluated from the slope and intercept of the von't Hoff plots (Fig. 15).

The pseudo-first and second-order equations of 0.1 g Fe_3O_4-WC and 25 and 50 mg L^{-1} solutions prepared in these analyzes were given in Table 5. The $\ln(q_e - q_t)$ line of the MB solution vs. time is shown in Figs. 16 and 17.

The linearity of the kinetic model was very important in deciding which model was suitable for the adsorption system. Depending on the fact that the R^2 value in the first-order equation was considerably lower than 1, it was concluded due to the fact that the R^2 value of the second-order equation was higher than 0.99, close to 1 and the amount of MB removed per adsorbent was greater than the first-order equation that, in order to elucidate the adsorption kinetics, the kinetic data were appropriate for the second-order kinetic model. Similar approaches were made in many studies in the literature for the adsorption of dyestuffs [41–45]. The q_e values obtained as a result of these studies, calculated velocity constants, and correlation coefficients are shown in Table 5.

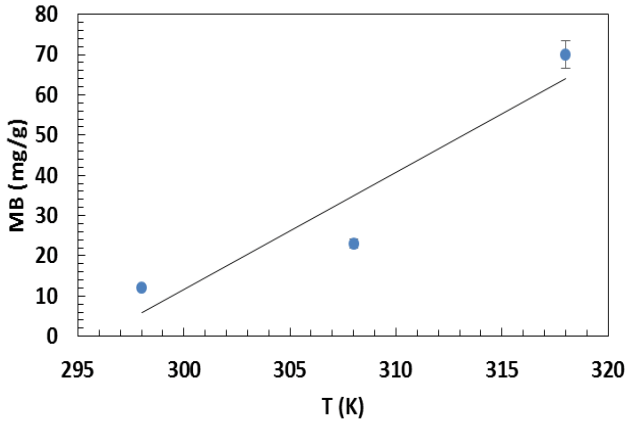

Fig. 14. Effect of temperature on the adsorption of MB.

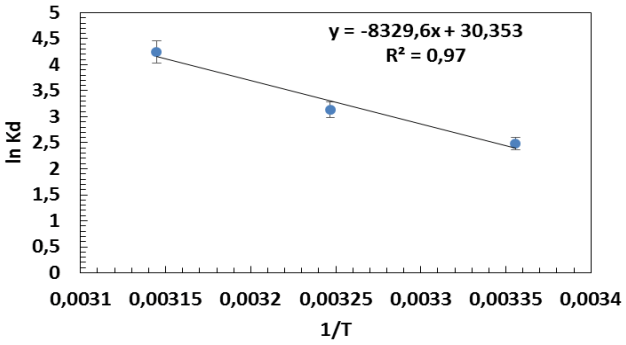

Fig. 15. 1/T vs. lnK_d.

Table 4
Comparison of MB adsorption among different adsorbent

Adsorbent	pH	Temperature (K)	Maximum adsorption capacity (mg g^{-1})	References
Fly ash	10.0	298	0.12	[11]
Fe_3O_4 at AC	10.0	298	138	[34]
Coconut shell	9.0	303	200.0	[35]
Pomegranate husks	6.0	3,188	36.90	[36]
Chitosan flakes-based AC	11.0	303	121.45	[37]
Pistachio shell-AC	4.2	298	129.0	[38]
Pumpkin seed shell	4.28	318	181.81	[39]
Euphorbia r-based AC	6.0	313	114.5	[40]
Fe_3O_4-WC	7.0	298	140.84	This study

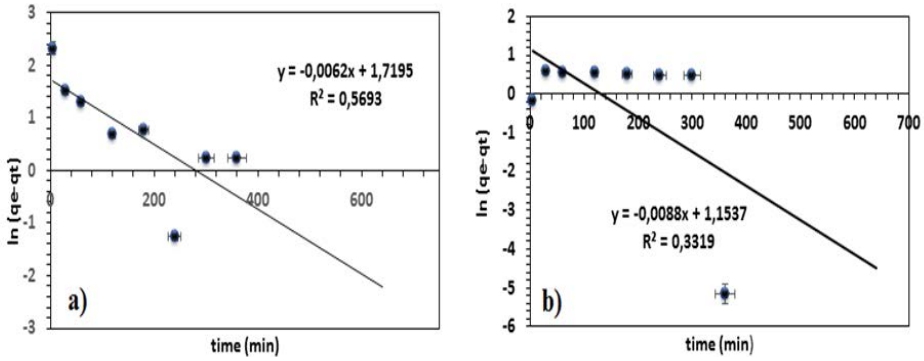

Fig. 16. Pseudo-first-order kinetic modeling results obtained for MB adsorption onto Fe_3O_4-WC composite (initial MB concentration: (a) 25 and (b) 50 mg L^{-1}, adsorbent dose: 0.1 g/100 mL, pH: 7.0, and temperature: 298 K).

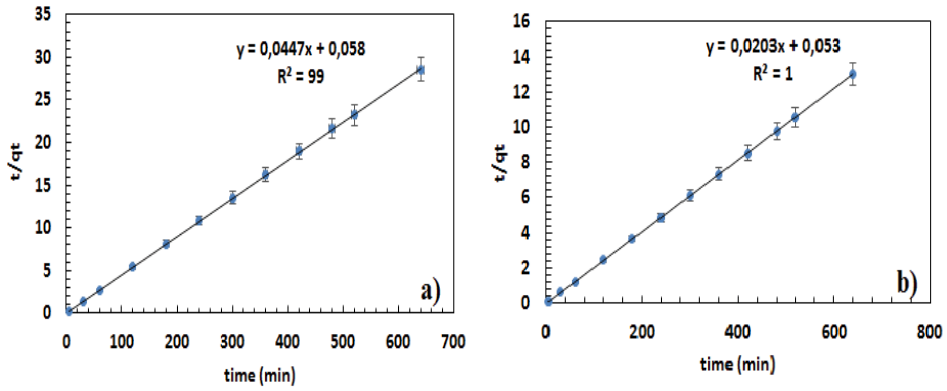

Fig. 17. Pseudo-second-order kinetic modeling results obtained for MB adsorption onto Fe_3O_4-WC composite (initial MB concentration: (a) 25 and (b) 50 mg L^{-1}, adsorbent dose: 0.1 g/100 mL, pH: 7.0, and temperature: 298 K).

3.9. Regeneration of the adsorbed MB from Fe_3O_4-WC sorbent

Desorption analyzes were performed with 0.1 g WC as well as 0.05 g, 0.1, 0.2 M NaOH solutions to recover MB adsorbed on wild chestnut and to understand the adsorption mechanism. After MB adsorption on Fe_3O_4-WC, cyclic desorption, and reusability were investigated. In order to reduce the use of the adsorbent, the adsorbent must have a reusable structure.

As can be seen from Fig. 18, the adsorption–desorption cycle was carried out seven times in the shaking system. No decrease in adsorption was observed during the studies. There was reduction of 14% in desorption in the 1st and 7th cycles. With this reduction, it was seen that WC was a suitable adsorbent to reuse. As a result of the processes, 63% of the MB was recovered, indicating its suitability to reuse. As shown in Fig. 18, the adsorption–desorption cycle was carried out seven times in a shaking system. There are similar studies in the literature [41,46–49].

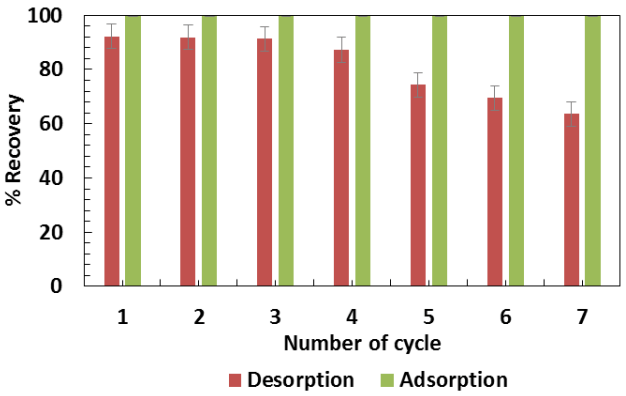

Fig. 18. Recycling efficiency of the Fe_3O_4-WC adsorbent prepared (temperature: 298 K, amount of adsorbent: 0.1 g/100 mL, stirring speed: 130 rpm, contact time: 640 min, and pH: 7.0).

4. Conclusions

In this study, in the first step, the outer shell of wild chestnut loaded magnetite Fe_3O_4 particles by using chemical precipitation method of Fe^{2+} and Fe^{3+}. In the second step, physicochemical properties and morphology of WC and Fe_3O_4-WC adsorbents, FTIR, XRD, and elemental analysis were made by SEM-EDS analysis techniques. As it was seen in SEM images, it was found to be successful in the adsorption process due to being porous and magnetic. The structure in the FTIR spectrum was found to be very rich in the functional group. The presence of Fe, Mg, O, P, Na, C, and Si was found in Fe_3O_4-WC samples. When XRD results were examined, it was found that the structure was amorphous and crystalline. In the third step, the feasibility

Table **5**
Parameters of the pseudo-first-order and the pseudo-second-order for MB adsorption

	Pseudo-first-order				Pseudo-second-order		
C_0 (mg L^{-1})	$q_{e,exp}$	k_1 (min^{-1})	$q_{e,cal}$ (mg g^{-1})	R^2	k_2 (g mg^{-1} min^{-1})	$q_{e,cal}$ (mg g^{-1})	R^2
25	22.14	0.014	52.42	0.57	0.77	22.37	0.99
50	49.20	0.020	14.24	0.33	0.38	49.26	1.00

of these sorbents for the removal of MB from aqueous solution was carried out by using the batch adsorption method. In the final stage, the experimental data were evaluated in terms of isotherm modeling, thermodynamic, and kinetic aspects. It was determined that optimum conditions for maximum adsorption has been pH 7, stirring time 240 min, adsorbent dosage 0.1 g/100 mL, and temperature 298 K.

The changing values of enthalpy ($\Delta H°$), entropy ($\Delta S°$), and Gibbs free energy ($\Delta G°$) in terms of the thermodynamic parameters of the adsorption process on the adsorbent were determined. A positive value of $\Delta H°$ indicated that the adsorption was endothermic. The positive value of $\Delta S°$ indicated that the irregularity increases at the solution–adsorbent interface during adsorption. A negative $\Delta G°$ value indicated that the methylene blue process from the solution on the adsorbent has occurred spontaneously.

According to experimental data, it was observed that our study was appropriate for the Langmuir isotherm. Under all circumstances of the study, the maximum adsorption capacity of MB on Fe_3O_4-WC was found to be 140.84 mg g^{-1}. The Langmuir isotherm R^2 value was greater than 0.95 showed that the chemical adsorption (complexation) was more effective in adsorption. The adsorption–desorption cycle was carried out in the shaking system by repeating seven times. It was seen that it had a high level of recovery performance even after the 7th cycle. As it was seen from the results, Fe_3O_4-WC samples can be used as eco-friendly, cost-efficient, and effective material for removing dyestuffs from wastewater due to the fact that they were effective in the removal of MB.

References

[1] N.T. Sheth, S.R. Dave, Optimisation for enhanced decolorization and degradation of Reactive Red BS C.I. 111 by *Pseudomonas aeruginosa* NGKCTS, Biodegradation, 20 (2009) 827–836.

[2] Y. Fu, T. Viraraghavan, Fungal decolorization of dye wastewaters, Bioresour. Technol., 79 (2001) 251–262.

[3] T. Robinson, G. McMullan, R. Marchant, P. Nigam, Remediation of dyes in textile effluent: a critical review on current treatment technologies with a proposed alternative, Bioresour. Technol., 77 (2001) 247–255.

[4] S.K. Matta, S. Agarwal, R. Bhatnagar, Surface localized and extracellular glyceraldehyde-3-phosphate dehydrogenase of *Bacillus anthracis* is a plasminogen binding protein, Biochim. Biophys. Acta, Proteins Proteomics, 1804 (2010) 2111–2120.

[5] A. Zille, F.D. Munteanu, G.M. Gübitz, A.C. Paulo, Laccase kinetics of degradation and coupling reactions, J. Mol. Catal. B: Enzym., 33 (2005) 23–28.

[6] A.S. Ozcan, A. Ozcan, Adsorption of acid dyes from aqueous solutions onto acid-activated bentonite, J. Colloids Interface Sci., 276 (2004) 39–46.

[7] P. Baskaralingam, M. Pulikesi, V. Ramamurthi, S. Sivanesan, Equilibrium studies for the adsorption of acid dye onto modified hectorite, J. Hazard. Mater., 136 (2006) 989–992.

[8] F. Akbal, Adsorption of basic dyes from aqueous solution onto pumice powder, J. Colloid Interface Sci., 286 (2005) 455–458.

[9] Z. Aksu, I.A. Isoglu, Use of agricultural waste sugar beet pulp for the removal of Gemozal turquoise blue-Greactive dye from aqueous solution, J. Hazard. Mater., 137 (2006) 418–430.

[10] M. Mahramanlıoğlu, I. Kizilcikli, I.O. Bicer, Adsorption of fluoride from aqueous solution by acid treated spent bleaching earth, J. Fluorine Chem., 115 (2002) 41–47.

[11] H. Karaca, E. Altıntıg, D. Türker, M. Teker, An evaluation of coal fly ash as an adsorbent for the removal of methylene blue from aqueous solutions: kinetic and thermodynamic studies, J. Dispersion Sci. Technol., 39 (2018) 1800–1807.

[12] M.A. Rauf, S.B. Bukallah, F.A. Hamour, A.S. Nasir, Adsorption of dyes from aqueous solutions onto sand and their kinetic behavior, Chem. Eng. J., 137 (2008) 238–243.

[13] Z. Aksu, S. Tezer, Biosorption of reactive dyes on the green alga *Chlorella vulgaris*, Process Biochem., 40 (2005) 1347–1361.

[14] K.C. Chen, J.Y. Wu, D.J. Liou, S.C. Hwang, Decolorization of the textile azo dyes by newly isolated bacterial strains, J. Biotechnol., 101 (2003) 57–68.

[15] J. Yener, T. Kopac, G. Dogu, T. Dogu, Adsorption of Basic Yellow 28 from aqueous solutions with clinoptilolite and amberlite, J. Colloid Interface Sci., 294 (2006) 255–264.

[16] N. Zaghbani, H. Amor, M. Dhahbi, Separation of Methylene Blue from aqueous solution by micellar enhanced ultrafiltration, Sep. Purif. Technol., 55 (2007) 117–124.

[17] S. Que, C. Papelis, A. Hanson, Predicting arsenate adsorption on iron-coated sand based on a surface complexation model, J. Environ. Eng., 139 (2013) 368–374.

[18] I. Hilbrandt, V. Lehmann, F. Zietzschmann, A.S. Ruhl, M. Jekel, Quantification and isotherm modelling of competitive phosphate and silicate adsorption onto micro-sized granular ferric hydroxide, RSC Adv., 9 (2019) 23642–23651.

[19] S.O. Chan, H.W. Cheung, G. McKay, Single and multicomponent acid dye adsorption equilibrium studies on tyre demineralised activated carbon, Chem. Eng. J., 191 (2012) 162–170.

[20] N. Kataria, V.K. Garg, Optimization of Pb(II) and Cd(II) adsorption onto ZnO nano flowers using central composites design: isotherms and kinetics modelling, J. Mol. Liq., 271 (2018) 228–239.

[21] N.M. Mahmoodi, R. Salehi, M. Arami, Binary system dye removal from colored textile wastewater using activated carbon: kinetic and isotherm studies, Desalination, 272 (2011) 187–195.

[22] K.A. Tan, N. Morad, T.T. Teng, I. Norli, P. Panneerselvam, Removal of cationic dye by magnetic nanoparticle (Fe_3O_4) impregnated onto activated maize cob powder and kinetic study of dye waste adsorption, APCBEE Procedia, 1 (2012) 83–89.

[23] E. Altıntıg, H. Altundag, M. Tuzen, A. Sarı, Effective removal of methylene blue from aqueous solutions using magnetic loaded activated carbon as novel adsorbent, Chem. Eng. Res. Des., 122 (2017) 151–163.

[24] L. Liu, Y. Lin, Y. Liu, H. Zhu, Q. He, Removal of Methylene Blue from aqueous solutions by sewage sludge based granular activated carbon: adsorption equilibrium, kinetics, and thermodynamics, J. Chem. Eng. Data, 58 (2013) 2248–2253.

[25] F. Zhang, J. Lan, Y. Yang, T. Wei, R. Tan, W. Song, Adsorption behavior and mechanism of methyl blue on zinc oxide

nanoparticles, J. Nanopart. Res., 15 (2013) 1–10, doi: 10.1007/s11051-013-2034-2.
[26] S. Karmaker, M.d.N. Uddin, H. Ichikawa, Y. Fukumori, T.K. Saha, Adsorption of reactive orange 13 onto jackfruit seed flakes in aqueous solution, J. Environ. Chem. Eng., 3 (2015) 583–592.
[27] N. Kataria, V.K. Garg, Green synthesis of Fe_3O_4 nanoparticles loaded sawdust carbon for Cadmium(II) removal from water: regeneration and mechanism, Chemosphere, 208 (2017) 818–828.
[28] L. Sun, S. Wan, W. Luo, Biochars prepared from anaerobic digestion residue, palm bark, and eucalyptus for adsorption of cationic methylene blue dye: characterization, equilibrium, and kinetic studies, Bioresour. Technol., 140 (2013) 406–413.
[29] S. Sivrikaya, H. Altundag, M. Zengin M. Imamoglu, Separation, preconcentration, and recovery of Pd(II) ions using newly modified silica gel with bis(3-aminopropyl)amine, Sep. Sci. Technol., 46 (2011) 2032–2040.
[30] M. Doğan, M. Alkan, Adsorption kinetics of methyl violet onto perlite, Chemosphere, 50 (2003) 517–528.
[31] C. Ozer, M. Imamoglu, Y. Turhan, F. Boysan, Removal of methylene blue from aqueous solutions using phosphoric acid activated carbon produced from hazelnut husks, Toxicol. Environ. Chem., 94 (2012) 1283–1293.
[32] P.E. Kumar, M. Santhi, Adsorption of rhodamine B from an aqueous solution: kinetic, equilibrium and thermodynamic studies, Int. J. Innovative Res. Sci. Eng. Technol., 4 (2015) 497–510.
[33] K. Siddique, M. Rizwan, M.J. Shahid, S. Ali, R. Ahmad, H. Rizvi, Textile wastewater Treatment Options: A Critical Review, N. Anjum, S. Gill, N. Tuteja, Eds., Enhancing Cleanup Environmental Pollutants, Springer, Cham, 2017, pp. 183–207.
[34] S. Joshi, V.K. Garg, N. Kataria, K. Kadirvelu, Applications of Fe_3O_4@AC nanoparticles for dye removal from simulated wastewater, Chemosphere, 236 (2019) 1–11, doi: 10.1016/j.chemosphere.2019.07.011.
[35] M.A. Islam, M.J. Ahmed, W.A. Khanday, M. Asif, B.H. Hameed, Mesoporous activated coconut shell-derived hydrochar prepared via hydrothermal carbonization-NaOH activation for methylene blue adsorption, J. Environ. Manage., 1 (2017) 237–244.
[36] N. Yilmaz, O. Alagoz, Adsorption of methylene blue on activated carbon prepared by chemical activation method from the pomegranate husks, ECJSE, 6 (2019) 817–829.
[37] F. Marrakchi, M.J. Ahmed, W.A. Khandaya, M. Asif, B.H. Hameed, Mesoporous-activated carbon prepared from chitosan flakes via single-step sodium hydroxide activation for the adsorption of methylene blue, Int. J. Biol. Macromol., 98 (2017) 233–239.
[38] A.A. Attia, B.S. Girgas, S.A. Khedr, Capacity of activated carbon derived from pistachio shells by H_3PO_4 in the removal of dyes and phenolics, J. Chem. Technol. Biotechnol., 78 (2003) 611–619.
[39] I. Demiral, A.C. Samdan, Removal of methylene blue with activated carbon obtained from pumpkin seed shell, J. Turk. Chem. Soc., 2 (2015) 25–28.
[40] O. Gerçel, A. Ozcan, A.S. Ozcan, H.F. Gerçel, Preparation of activated carbon from a renewable bio-plant of *Euphorbia rigida* by H_2SO_4 activation and its adsorption behavior in aqueous solutions, Appl. Surf. Sci., 253 (2007) 4843–4852.
[41] E. Altıntığ, M. Onaran, A. Sarı, H. Altundag, M. Tuzen, Preparation, characterization and evaluation of bio-based magnetic activated carbon for effective adsorption of malachite green from aqueous solution, Mater. Chem. Phys., 220 (2018) 313–321.
[42] M. Ghaedi, A. Ansari, M.H. Habibi, A.R. Asghari, Removal of malachite green from aqueous solution by zinc oxide nanoparticle loaded on activated carbon: kinetics and isotherm study, J. Ind. Eng. Chem., 20 (2014) 17–18.
[43] Z. Pan, S. Wang, Y. Liu, B. Li, Z. Jia, Y. Zhang, J. Wang, The hydration, pore structure and strength of cement-based material prepared with waste soaking solution from acetic acid treatment of regenerated aggregates, J. Cleaner Prod., 235 (2019) 866–874.
[44] M. Naushad, G. Sharma, Z.A. Alothman, Photodegration of toxic dye using gum Arabic-crosslinked poly (acrylamide)/$Ni(OH)_2$/FeOOH nanocomposites hydrogel, J. Cleaner Prod., 241 (2019) 1–9, doi: 10.1016/j.jclepro.2019.118263.
[45] N. Subedi, A. Lähde, E. Abu-Danso, J. Iqbal, A. Bhatnagar, A comparative study of magnetic chitosan (Chi@Fe_3O_4) and graphene oxide modified magnetic chitosan (Chi@Fe_3O_4GO) nanocomposites for efficient removal of Cr(VI) from water, Int. J. Biol. Macromol., 137 (2019) 948–959.
[46] J. Iqbal, N.S. Shah, M. Sayed, N. Muhammad, S. Rehman, J.A. Khan, Z.U.H. Khan, F.M. Howari, Y. Nazzal, C. Xavier, S. Arshad, A. Hussein, K. Polychronopoulou, Deep eutectic solvent-mediated synthesis of ceria nanoparticles with the enhanced yield for photocatalytic degradation of flumequine under UV-C, J. Water Process Eng., 33 (2020) 1–13, doi: 10.1016/j.jwpe.2019.101012.
[47] A. Maged, J. Iqbal, S. Kharbish, I.S. Ismael, A. Bhatnagar, Tuning tetracycline removal from aqueous solution onto activated 2:1 layered clay mineral: characterization, sorption and mechanistic studies, J. Hazard. Mater., 384 (2020) 1–13, doi: 10.1016/j.jhazmat.2019.121320.
[48] M. Naushad, A.A. Alqadami, Z.A. AlOthman, I.H. Alsohaimi, M.S. Algamdi, A.M. Aldawsari, Adsorption kinetics, isotherm and reusability studies for the removal of cationic dye from aqueous medium using arginine modified activated carbon, J. Mol. Liq., 293 (2019) 1–7, doi: 10.1016/j.molliq.2019.111442.
[49] S. Joshi, V.K. Garg, J. Saini, K. Kadirvelu, Removal of toulidine blue O dye from aqueous solution by silica-iron oxide nanoparticles, Mater. Focus, 7 (2018) 146–147.